Investigation of the spin-lattice coupling in $Mn_3Ga_{1-x}Sn_xN$ antiperovskites

Kewen Shi,[1,2,3] Ying Sun,[1,*] Claire V. Colin,[2,3] Lei Wang,[1] Jun Yan,[1] Sihao Deng,[1] Huiqing Lu,[1] Wenjun Zhao,[1] Yamaura Kazunari,[4,5] Pierre Bordet,[2,3] and Cong Wang[1,†]

[1]*Center for Condensed Matter and Materials Physics, Department of Physics, Beihang University, Beijing 100191, People's Republic of China*
[2]*CNRS, Institut NEEL, F-38000 Grenoble, France*
[3]*Université Grenoble Alpes, Institut NEEL, F-38000 Grenoble, France*
[4]*Research Center for Functional Materials, National Institute for Materials Science (NIMS), 1-1 Namiki, Tsukuba, Ibaraki 305-0044, Japan*
[5]*Graduate School of Chemical Sciences and Engineering, Hokkaido University, North 10 West 8, Kita-ku, Sapporo, Hokkaido 060-0810, Japan*

(Received 20 September 2017; revised manuscript received 1 December 2017; published 20 February 2018)

The magnetovolume effects (MVEs) of $Mn_3Ga_{1-x}Sn_xN$ antiperovskite compounds have been investigated by means of neutron powder diffraction. Increasing the Sn-doping content at the Ga site leads to the broadening of the magnetic phase transition temperature range and the thermal expansion behavior changes from negative to positive. We establish the relationship between the square of the ordered magnetic moment m^2 and the volume variation $\Delta\omega_m$ for the antiferromagnetic phase (Γ^{5g} magnetic structure with rhombohedral symmetry $R\bar{3}m$). The temperature variations of $\Delta\omega_m(T)$, $m^2(T)$ and the magnetoelastic coupling constant $C(T)$ are also quantitatively analyzed according to the itinerant-electron theory. Moreover, the increase of the phonon contribution to the thermal expansion induced by Sn doping and the corresponding decrease of dm/dT are revealed to be the key parameters for tuning the MVEs. Our results allow elucidating and quantifying the mechanism of the spin-lattice coupling and can be used to design magnetic functional materials with controlled thermal expansion behaviors for specific applications.

DOI: 10.1103/PhysRevB.97.054110

I. INTRODUCTION

Normally, solid materials expand on heating and contract on cooling. That is to say, the coefficient of thermal expansion (CTE), $\beta = \frac{1}{V_0}(\frac{\partial V}{\partial T})_p$, should be positive. However, some solid materials display anomalous thermal expansion [1,2], i.e., negative thermal expansion (NTE) or zero thermal expansion (ZTE), in which cases the CTE is negative or near zero, respectively. So far, four different mechanisms have been identified to explain these phenomena, depending on the type of material, including the (1) special phonon vibration model in ZrW_2O_8 [2] and ScF_3 [3]; (2) magnetovolume effect (MVE) in $MnCo_{1-x}Ge_x$ [4], Fe-Ni Invar alloys [5,6], and R_2Fe_{17} (R is rare earth) [7,8]; (3) electron transfer in $LaCu_3Fe_4O_{12}$ [9], $BiNiO_3$ [10], and the MgB_2 superconductor [11]; (4) ferroelectric effect in $PbTiO_3$-based ferroelectrics [12–14] and $Sn_2P_2S_6$ [15]. MVE was shown to be responsible for negative/zero thermal expansion behaviors in antiperovskite compounds Mn_3MX (M = Ga, Zn, Cu, Sn; X = C, N) [16–19], in relation to their strong "spin-lattice" coupling. As a consequence of this strong spin-lattice coupling, antiperovskite materials display many interesting physical properties, such as the barocaloric effect [20], baromagnetic effect [21], piezomagnetic effect [22], magnetocaloric effect [23], magnetoresistance [24], and the near-zero temperature coefficient of resistivity [25], and are therefore becoming important candidates for designing smart materials and functional devices/sensors [26]. Unfortunately, a quantitative relationship between lattice variation and spin ordering is still lacking. In this work, we will investigate this coupling and present a detailed quantitative description of the temperature variation of the magnetovolume effect in $Mn_3Ga_{1-x}Sn_xN$ compounds using neutron powder diffraction (NPD).

II. EXPERIMENT

Polycrystalline samples $Mn_3Ga_{1-x}Sn_xN$ were prepared by a solid-state reaction using fine Mn_2N powders, Ga (4N) pellets, and Sn (4N) powders as starting materials. Mn_2N powder was synthesized by sintering Mn powder (4N) in nitrogen gas flow at 800 °C for several days [27]. Stoichiometric amounts of Mn_2N powder and Ga pellets were first sintered for 2 h, as previously reported [21]. Then, after thoroughly mixing with Sn powders by mechanical grinding, the samples were pressed into pellets, sealed under vacuum (10^{-5} Pa) in a quartz tube, and sintered at 800 °C for several days.

X-ray diffraction (XRD) patterns at room temperature were obtained with an X'Pert PRO powder diffractometer using Cu K_α radiation. The linear thermal expansion behaviors of the samples were measured with a heating rate of 5 K/min from 123 to 470 K (from 123 to 600 K for $Mn_3Ga_{0.1}Sn_{0.9}N$), using a Netzsch DIL 402C apparatus. The temperature dependence of magnetization was measured between 5 and 800 K under a magnetic field of 100 Oe and 10 kOe using a Quantum Design Magnetic Property Measurement System (MPMS). The measurements were carried out under field-cooling conditions for cooling (FCC) and warming (FCW). Isothermal magnetization curves were recorded between −70 and 70 kOe using the

*sunying@buaa.edu.cn
†congwang@buaa.edu.cn

same MPMS, while the isothermal magnetization curve for $Mn_3Ga_{0.5}Sn_{0.5}N$ between −50 and 50 kOe was obtained by using Quantum Design superconducting quantum interference device (5T-SQUID).

Neutron powder diffraction (NPD) data were collected using the two-axis diffractometer D1B at the Institut Laue-Langevin (ILL) with a neutron wavelength 1.2892 Å in the temperature range 10–550 K. The crystal and magnetic structures were refined with the Rietveld method using the FULLPROF suite programs [28] The neutron scattering lengths used were −0.3730, 0.7288, 0.6225, and 0.9360 ($\times 10^{-12}$ cm) for Mn, Ga, Sn, and N, respectively.

III. RESULTS AND DISCUSSION

We first report the analysis of the crystal and magnetic structures of $Mn_3Ga_{1-x}Sn_xN$ ($x = 0.1$, 0.3, 0.5, 0.7, or 0.9) compounds. Inspection of the room-temperature XRD patterns (shown in the Supplemental Material [29]) indicates that the main phase of all synthesized samples adopts the cubic perovskite structure with space group $Pm\bar{3}m$. As the Sn-doping content (x) increases, the lattice constants and unit-cell volumes increase linearly, in agreement with the Vegard's law [30], indicating that Sn has been successfully substituted to Ga in our samples. To determine the magnetic structures, the NPD patterns at 10 K of the $Mn_3Ga_{1-x}Sn_xN$ ($x = 0.1$, 0.7, 0.9) compounds were analyzed. Figures 1(a)–1(c) show the corresponding Rietveld plots for the refined crystal and magnetic structures. In order to highlight the magnetic contribution at 10 K, Fig. 1(d) shows the difference patterns (I_{obs}–I_{cal}) obtained by fitting the $Mn_3Ga_{0.9}Sn_{0.1}N$ NPD data including either only nuclear scattering or both nuclear and magnetic scattering. The cubic perovskite structure with space group $Pm\bar{3}m$ was found to describe well the crystal structure, while all the magnetic reflections could be indexed with the magnetic propagation vector $k = (0, 0, 0)$. Magnetic symmetry analysis was carried out using the program K-SUBGROUPSMAG from the Bilbao Crystallographic Server [31]. Rietveld refinements indicated that the best magnetic model is the maximum magnetic rhombohedral subgroup $R\bar{3}m$ within the irreducible magnetic representation Γ^{5g}. The corresponding Γ^{5g} magnetic structure [32] is shown in the inset of Fig. 1(a). The orientation of the Mn spins forming a triangle within the (111) planes rotate by 120°, leading to a zero magnetic moment for each plane. In adjacent planes, the spins rotate in opposite directions. The refined magnetic moments for Mn are 2.31(2), 2.41(3), and 2.43(3) μ_B, for $x = 0.1$, 0.7, and 0.9, respectively. The refined compositions of the $x = 0.7$ and $x = 0.9$ compounds were determined to be $Mn_3Ga_{0.33(5)}Sn_{0.67(5)}N_{0.93(2)}$ and $Mn_3Ga_{0.14(9)}Sn_{0.86(9)}N_{0.89(3)}$ by fixing the Mn content at 3 in the refinements of the NPD patterns at 550 K. The composition of the $x = 0.1$ compound was found to be $Mn_3Ga_{0.90(2)}Sn_{0.10(2)}N$ by Rietveld refinement of the XRD pattern at room temperature, as shown in the Supplemental Material [29]. Here the Mn and N contents were fixed at 3 and 1, respectively. The refined stoichiometries of the three samples are thus quite close to the nominal compositions. Additional refined structural parameters for the NPD refinements are shown in Table I. Several peaks

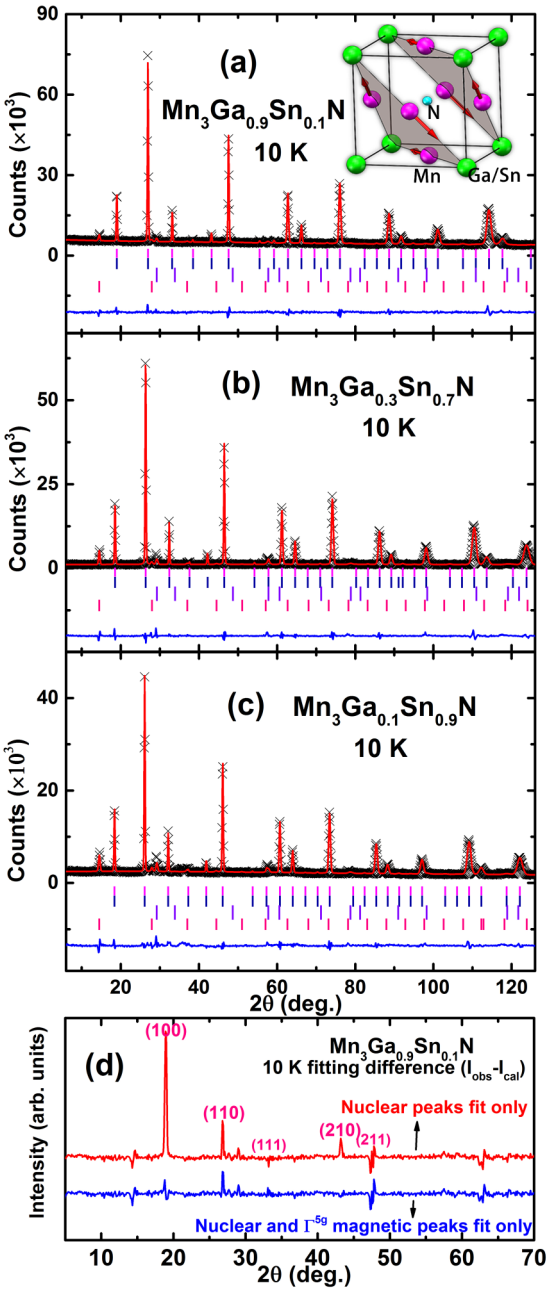

FIG. 1. (a)–(c) NPD refinement plots for the $Mn_3Ga_{1-x}Sn_xN$ ($x = 0.1$, 0.7, 0.9) compounds at 10 K. The crosses show the experimental intensities (I_{obs}), the upper solid line shows the calculated intensities (I_{calc}), and the lower solid line is the difference between the observed and calculated intensities ($I_{obs} - I_{calc}$). The vertical bars mark the angular positions of the nuclear (the first and third rows) and magnetic (the second and fourth rows) Bragg reflections. (The first and second rows are for $Mn_3Ga_{1-x}Sn_xN$; the third and fourth rows are for MnO.) The inset gives the magnetic structure of $Mn_3Ga_{1-x}Sn_xN$, corresponding to rhombohedral ($R\bar{3}m$) magnetic symmetry. (d) The solid lines show the differences (I_{obs}–I_{cal}) generated by fitting the data with only nuclear (top) or with nuclear and magnetic (bottom) for $Mn_3Ga_{0.9}Sn_{0.1}N$ at 10 K, respectively. The magnetic contribution of the Γ^{5g} structure to the patterns is clearly visible.

corresponding to the crystal and magnetic structures of an MnO impurity phase can be observed in the NPD as well as XPD patterns (Fig. 1). The presence of this minor phase (with a Neel

TABLE I. Agreement factors and refined structural parameters for $Mn_3Ga_{1-x}Sn_xN$ compounds from Rietveld refinement of NPD data in the paramagnetic phases.

Sample Formula		$Mn_3Ga_{0.9}Sn_{0.1}N$	$Mn_3Ga_{0.33(5)}Sn_{0.67(5)}N_{0.93(2)}$	$Mn_3Ga_{0.14(9)}Sn_{0.86(9)}N_{0.89(3)}$
Temperature		500 K	550 K	550 K
a (Å)		3.91731(6)	4.02097(6)	4.05930(9)
V (Å^3)		60.112(2)	65.012(2)	66.889(3)
	Mn (3c)	0.54(6)	0.77(9)	0.9(2)
B (Å^2)	Ga/Sn (1a)	0.51(5)	0.57(7)	0.7(1)
	N (1b)	0.16(5)	0.27(7)	0.4(1)
R_{wp} (%)		6.59	3.85	8.33
R_{Bragg} (%)		4.01	2.85	5.07
χ^2		14.1	7.98	11.5
MnO phase fraction (wt %)		4.1(2)	5.1(2)	11.7(7)

temperature of about 110 K) does not noticeably influence our results or the discussion presented below on the properties in these antiperovskite compounds.

Since the anomalous thermal expansion behaviors in antiperovskite compounds are always correlated with a magnetic transition, we first present a detailed analysis of the magnetic properties. As shown in Figs. 2(a)–2(c), an antiferromagnetic (AFM) transition is observed at $T_N = 320$ K (FCC at 100 Oe) for $Mn_3Ga_{0.9}Sn_{0.1}N$, which is higher than the Néel temperature of 298 K in the Mn_3GaN host material [16,33]. For $x = 0.3$, the corresponding Néel temperature appears at 392 K in the FCW curve at 100 Oe and 390 K in the FCC curve at 10 kOe. With increasing Sn content x, the AFM transition temperature increases further, to 480 K for $x = 0.5$, 499 K for $x = 0.7$, and 529 K for $x = 0.9$ (FCW at 100 Oe), respectively. For $x = 0.7$ and 0.9, a new magnetic transition from the AFM phase to a weak ferromagnetic phase appears at 39 and 48 K on cooling, respectively. This is confirmed in the isothermal magnetization

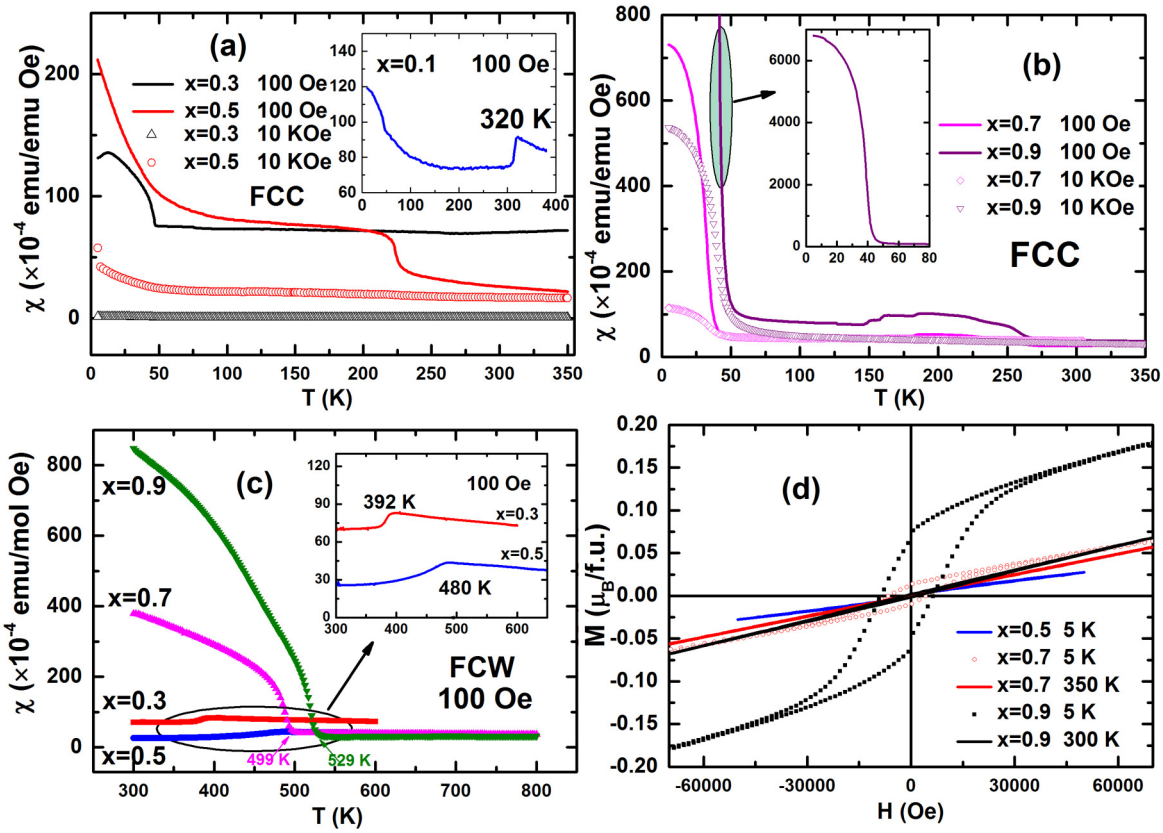

FIG. 2. (a) Temperature dependence of magnetization (FCC) of (a) $Mn_3Ga_{0.7}Sn_{0.3}N$ and $Mn_3Ga_{0.5}Sn_{0.5}N$, (b) $Mn_3Ga_{0.3}Sn_{0.7}N$ and $Mn_3Ga_{0.2}Sn_{0.9}N$ compounds from 5 to 350 K under 100 Oe and 10 kOe applied magnetic field. The inset of the graph (a) shows the magnetization curve of $Mn_3Ga_{0.9}Sn_{0.1}N$ at 100 Oe. (c) Temperature dependence of magnetization (FCW at 100 Oe) of $Mn_3Ga_{1-x}Sn_xN$ compounds from 300 to 800 K. The inset shows the enlarged magnetization curve of $x = 0.3$ and 0.5 at 100 Oe. (d) The isothermal magnetization of the $Mn_3Ga_{1-x}Sn_xN$ compounds.

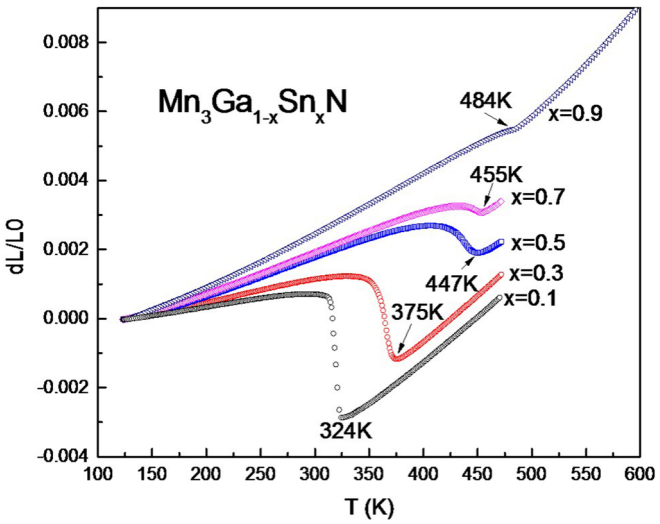

FIG. 3. Linear thermal expansion [dL/L_0 (123 K); $dL = L–L_0$ (123 K)] of $Mn_3Ga_{1-x}Sn_xN$ compounds. L_0 (123 K) represents the length at 123 K for these samples.

curves of Fig. 2(d). For both compounds, the M-H curve at 5 K exhibits a hysteretic loop characteristic of a ferromagnetic contribution. However, the highest spontaneous magnetization is about 0.08 μ_B/f.u., i.e., ~0.027 μ_B/Mn atom for $x = 0.9$ and such a weak FM component can hardly be detected by NPD. As shown by the difference plots of the NPD patterns at 10 K (15 K) and 300 K for $Mn_3Ga_{0.3}Sn_{0.7}N$ and $Mn_3Ga_{0.1}Sn_{0.9}N$ in the Supplemental Material [29], only the effects of the lattice constant evolution and saturation of the ordered magnetic moment can be observed, which indicates that the Γ^{5g} AFM magnetic structure is preserved in the whole temperature range of magnetic order. The calculation of the piezomagnetic effect in Mn_3GaN [22] indicated that the strain forces may be responsible for the rotation of the Mn spins out of the (111) plane, leading to a net ferromagnetic component at low temperature. This effect could be at the origin of the weak ferromagnetic moment obtained by the magnetization measurements.

The thermal expansion dL/L_0 (123 K) of the $Mn_3Ga_{1-x}Sn_xN$ compounds is shown in Fig. 3. Previous work [16,33] reported that pure Mn_3GaN undergoes a magnetic phase transition from the Γ^{5g} AFM phase to the paramagnetic (PM) phase accompanied by a sharp volume contraction of ~1% at 298 K. The results shown in Fig. 3 indicate that Sn doping from $x = 0.1$ to 0.9 efficiently increases the responding temperature of the magnetovolume anomaly from 324 to 484 K, while decreasing the magnitude of the volume contraction from ~3.5% to nearly 0. For the $Mn_3Ga_{0.1}Sn_{0.9}N$ compound, at the transition temperature of 484 K, we can only observe a change of linear thermal expansion coefficient α without a detectable NTE effect. It is also worth noting that below T_N, the value of α increases with increasing Sn content. This indicates that the magnetovolume effect can be effectively tuned by Sn doping in $Mn_3Ga_{1-x}Sn_xN$ compounds.

In order to clarify the spin-lattice coupling and the thermal expansion mechanism in $Mn_3Ga_{1-x}Sn_xN$ compounds, NPD patterns were collected at variable temperature and analyzed by Rietveld refinement. The temperature dependence of the lattice constants a and magnetic moments m of $Mn_3Ga_{1-x}Sn_xN$

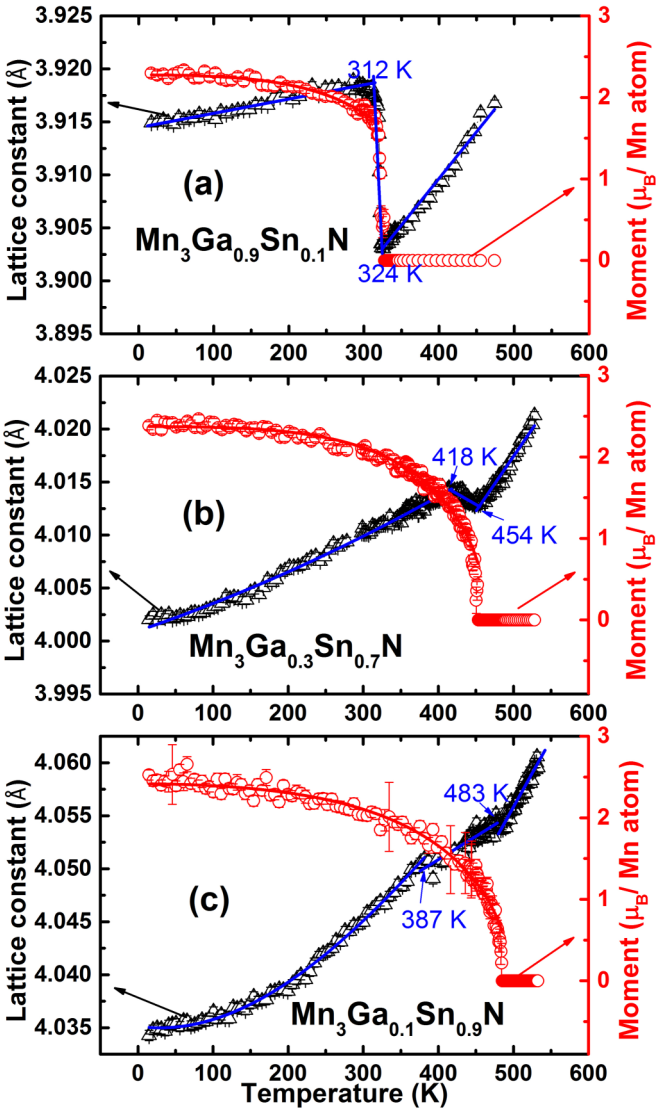

FIG. 4. (a)–(c) Temperature variations of the lattice constants a and magnetic moments m of $Mn_3Ga_{1-x}Sn_xN$ ($x = 0.1$, 0.7, 0.9) compounds. The red solid lines represent the fits of the magnetic moment dependences using the formula $m^2(T) = m^2(0)[1 - \alpha(\frac{T}{T_N})^2 + \xi(\frac{T}{T_N})^4]$. The blue lines are *a(T)* fits used to determine the reported transition temperatures.

($x = 0.1$, 0.7, 0.9) compounds are shown in Figs. 4(a)–4(c). It is clear that only a single magnetic phase transition from AFM to PM can be detected over the whole temperature range. This transition is accompanied by a strong magnetovolume effect as seen from the unit-cell parameter variation, but the antiperovskite structural arrangement remains unchanged. As shown by the solid lines in Fig. 4, the temperature dependence of the magnetic moment could be well fitted by the formula $m^2(T) = m^2(0)[1 - \alpha(\frac{T}{T_N})^2 + \xi(\frac{T}{T_N})^4]$, which will be discussed further in the following. On heating, the phase transitions are accopanied by a lattice contraction (NTE behavior) for $x = 0.1$, 0.7 and a steplike lattice variation (PTE behavior) for $x = 0.9$ at the Néel temperature. For $x = 0.1$, the behavior is typical of a first-order phase transition, with an abrupt drop of lattice constant and magnetic moment. As seen in Fig. 4(a),

TABLE II. Thermal expansion parameters at the transition temperature and parameters obtained by fitting the *V(T)* curves with the Debye model for $Mn_3Ga_{1-x}Sn_xN$ ($x = 0.1$, 0.7, and 0.9).

$Mn_3Ga_{1-x}Sn_xN$	Temperature range for phase transition (K)	CTE ($\times 10^{-6}$ /K)	V_0 (Å^3)	$9\gamma Nk_B/B$ (Å^3/K)	Θ_D (K)
$x = 0.1$	$312 \sim 324$ ($\Delta T = 12$)	−139.3	58.92(2)	0.0158(6)	893(33)
$x = 0.7$	$418 \sim 454$ ($\Delta T = 36$)	−8.1	63.10(5)	0.0197(9)	788(53)
$x = 0.9$	$387 \sim 483$ ($\Delta T = 96$)	11.2	64.60(7)	0.0202(9)	583(61)

the NTE temperature range is quite narrow, from 312 to 324 K (the phase transition temperatures were determined by the crossing of the fitting lines of *a-T* curves shown in Fig. 4). With increasing Sn content to $x = 0.7$, the temperature range where NTE takes place has broadened to 36 K (from 418 to 454 K), and the decrease of the ordered magnetic moment in the Γ^{5g} AFM phase also becomes smoother. With further increase of the Sn content to $x = 0.9$, only a change of slope in the lattice constant is observed without sizeable NTE behavior, although the Γ^{5g} phase still exists. At the same time, the phase transition temperature range is broadened to 96 K (from 387 to 483 K). These results, summarized in Table II, indicate that Sn doping increases the Néel temperature, broadens the NTE temperature range, decreases the value of dm/dT close to the transition points, and tunes the thermal expansion from negative (−139.3 and −8.1 ppm/K for $x = 0.1$, 0.7, respectively) to positive (11.2 ppm/K for $x = 0.9$).

The anomalous thermal expansion behaviors in antiperovskites are considered to originate from strong magnetic correlations and lattice vibrations. Generally, the (normally positive) thermal expansion behavior due to the phonon contributions is theoretically estimated by using the Debye equation [34,35]:

$$V_p \cong V_0 + \frac{9\gamma Nk_B}{B} T \left(\frac{T}{\Theta_D}\right)^3 \int_0^{\Theta_D/T} \frac{x^3}{e^x - 1} dx, \quad (1)$$

where V_0, γ, B, and Θ_D represent the volume at 0 K (considering phonon contribution only), the Grüneisen parameter, the bulk modulus, and the Debye temperature, respectively. As is well known, the Debye model is a rather good and simple quasiharmonic approximation for describing the contribution of the lattice vibrations to the thermal expansion of solid crystals, although the anharmonic terms are neglected [36]. This model is suitable for many simple compounds and elements not only in cubic systems but also for some lower symmetries [37]. Although the accurate details of anharmonic phonons are missed, this approximation is also widely used to describe the thermal expansion behavior in various classes of materials, such as in $Na_2Ca_3Al_2F_{14}$ (often used as the calibration of XRD and NPD) [38], perovskites compounds [34,39,40], Invar alloys [41], and garnets [42]. Therefore, we have applied the Debye model to carry out with Eq. (1) a least-squares fit of the *V(T)* curves in the paramagnetic domain for the $x = 0.1$, 0.7, and 0.9 samples. The best fits are represented by dotted lines in Fig. 5(a), expressing the contribution of the phonons to the thermal expansion, while neglecting the magnetic excitations or spin fluctuations effects [40,43]. The V_0, $9\gamma Nk_B/B$, and Θ_D refined parameters are shown in Table II.

Furthermore, by subtracting to the experimental $V(T)$ curve this modeled phonon contribution extrapolated to the magnetic ordered phase domain, an extra contribution is obtained, which can be of magnetic or electronic origin where the magnetophonon or the electron-phonon interactions cannot be taken into consideration by doing this separation in phenomenology. Here, the magnetic contributions to the volumes in $Mn_3Ga_{1-x}Sn_xN$ can be safely considered as the key factor for the thermal expansion anomaly. Thus, it can be obtained by the difference between the measured volume V and

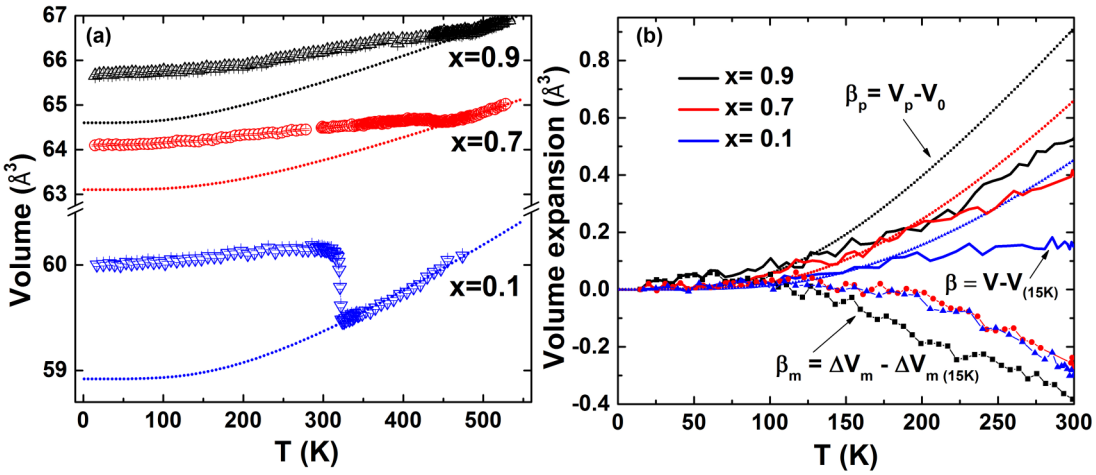

FIG. 5. (a) Temperature dependence of the unit-cell volume of the $Mn_3Ga_{1-x}Sn_xN$ ($x = 0.1, 0.7, 0.9$) compounds. The dotted lines represent the contribution of the phonon fitted by the Debye function. (b) Temperature dependence of the isotropic volume expansion $\beta = V - V_{(15K)}$ (solid lines), phonon contribution $\beta_p = V_p - V_0$ (dotted lines), and magnetic contribution $\beta_m = \Delta V_m - \Delta V_{m(15K)}$ (solid lines with symbols) for $Mn_3Ga_{1-x}Sn_xN$ compounds (blue: $x = 0.1$; red: $x = 0.7$; black: $x = 0.9$).

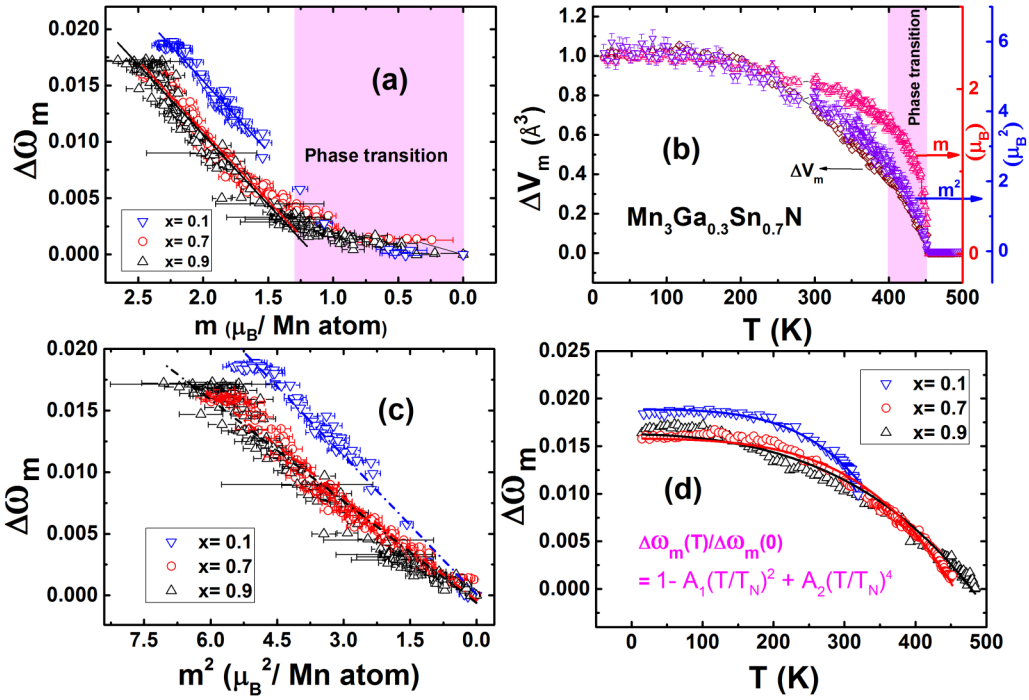

FIG. 6. (a) Volume strain $\Delta\omega_m$ induced by the magnetovolume effect as a function of magnetic moment m for $Mn_3Ga_{1-x}Sn_xN$ ($x = 0.1$, 0.7, 0.9) compounds. The solid lines correspond to linear fittings above the phase transition temperature. (b) Temperature dependence of ΔV_m (left), magnetic moment m (right), and the square of the magnetic moment m^2 (right) for $Mn_3Ga_{0.3}Sn_{0.7}N$. (c) Volume strain $\Delta\omega_m$ as a function of the square of the magnetic moment m^2 for $Mn_3Ga_{1-x}Sn_xN$ ($x = 0.1, 0.7, 0.9$) compounds. The dash-dotted lines correspond to linear fittings. (d) Temperature dependence of volume strain $\Delta\omega_m$ for $Mn_3Ga_{1-x}Sn_xN$ ($x = 0.1, 0.7, 0.9$) compounds with the fitted solid lines by the equation $\Delta\omega_m(T)/\Delta\omega_m(0) = 1 - A_1(T/T_N)^2 + A_2(T/T_N)^4$.

the calculated phonon contribution V_p, i.e., $\Delta V_m = V - V_p$. Therefore, we can discuss the separated phonon and magnetic contributions to the whole volume expansions. In Fig. 5(b), the isotropic volume expansion $\beta = V - V_{(15K)}$, the phonon contribution $\beta_p = V_p - V_0$, and the magnetic contribution $\beta_m = \Delta V_m - \Delta V_{m(15K)}$ below 300 K are represented for the $Mn_3Ga_{1-x}Sn_xN$ compounds ($x = 0.1$, 0.7, 0.9). Clearly, Sn doping strongly increases the phonon contribution and also the expansion coefficient below the phase transition. Comparing the results for $x = 0.1$ and $x = 0.7$, although the magnetic contributions β_m are very close, the isotropic volume expansion β for $x = 0.7$ is still larger than that for $x = 0.1$ due to the increase of the phonon contribution. When the temperature is below 225 K, the magnetic contribution β_m for $x = 0.9$ is quite larger than that for $x = 0.7$, while β for $x = 0.9$ is still slightly larger than that for $x = 0.7$. Below the transition temperature, the value of the volume expansion β exhibits the same tendency as the phonon contribution β_p, which means that the phonon contribution is the key factor which controls the CTE of the thermal expansion behavior. Besides the effect of phonons, the magnetic contribution, especially the rate of the temperature dependence of magnetic moment, also plays an important role in the change of sign of the thermal expansion anomaly from negative to positive and also in the broadening of the phase transition.

On the other hand, ΔV_m as well as the ordered magnetic moment decrease slightly with increasing temperature, which indicates a significant coupling between the magnetic moments and the lattice. As already reported in Ref. [44], investigations based on NPD data revealed that the ratio $r(T) = \Delta a_m(T)/m_{NTE}(T)$ for the Γ^{5g} phase below the magnetic transition temperature is approximately independent of T, which leads to a linear relationship between $\Delta a_m(T)$ and the ordered moment $m_{NTE}(T)$. However, when the magnetic phase transition gradually transforms from first order to second order, i.e., the anomalous (negative) thermal expansion behavior near the transition has become broader, this quantitative relationship between the volume strain $\Delta\omega_m$ and the magnetic moment m is no longer suitable and needs to be further developed for the whole temperature domain of the Γ^{5g} AFM phase, as the $\Delta\omega_m = \frac{\Delta V_m}{V_p}$ vs m plots shown in Fig. 6(a). Indeed, we could obtain a satisfactory agreement by considering the variation of volume strain $\Delta\omega_m$ vs m^2(= the square of the orderedmagnetic moment). The temperature dependence of ΔV_m, m, and m^2 for $Mn_3Ga_{0.3}Sn_{0.7}N$ are plotted together in Fig. 6(b). The variations of these three sets of values are approximately similar at low temperature. However, at higher temperature in the transition domain, the agreement is much better as a function of m^2 than of m. Thus, we will consider the former to establish a new quantitative relationship for spin-lattice coupling. As shown in Fig. 6(c), we obtain a satisfactory linear fit of $\Delta\omega_m$ as a function of the square of the ordered magnetic moment m^2, i.e., $\Delta\omega_m \propto m^2$, where the slope of the fitting curves is obtained to be 0.00375(3), 0.00278(3), and 0.00275(3) $\mu_B{}^{-2}$ for $x = 0.1$, 0.7 and 0.9, respectively, as shown in Table III.

Generally, in the framework of the Stoner-Wohlfarth (SW) theory [45–47] of the itinerant-electron magnetism (not only

TABLE III. Parameters obtained by fitting Eqs. (2), (6), (7), and (8) to NPD measurement data to clarify the mechanism of the magnetovolume effect in $Mn_3Ga_{1-x}Sn_xN$ compounds.

$Mn_3Ga_{1-x}Sn_xN$	$x = 0.1$	$x = 0.7$	$x = 0.9$
T_N	327 K	453 K	485 K
$M(0)$	2.28(1) μ_B	2.37(1) μ_B	2.42(1) μ_B
α	0.15(7)	0.12(4)	0.44(5)
ξ	−0.35(7)	−0.79(4)	−0.50(6)
$\Delta\omega_m(0)$	0.01888(9)	0.01579(8)	0.0162(1)
A_1	0.069(7)	0.202(6)	0.61(1)
$A_2 = (\alpha A_1 + \xi - \alpha^2)$	−0.34	−0.78	−0.43
$\gamma = A_1 - \alpha$	0.081	0.082	0.17
$C(0) = \Delta\omega_m(0)/M(0)^2$	0.00363 $\mu_B{}^{-2}$	0.00281 $\mu_B{}^{-2}$	0.00277 $\mu_B{}^{-2}$
C [treated as a constant in Eq. (3)]	0.00375(3) $\mu_B{}^{-2}$	0.00278(3) $\mu_B{}^{-2}$	0.00275(3) $\mu_B{}^{-2}$

ferromagnets [46,47] but also antiferromagnets [48–50]), the spontaneous volume magnetostriction can be expressed as the well-known equation

$$\Delta\omega_m(T) = CM^2(T), \tag{2}$$

where $C(=D/B)$ is the magnetoelastic coupling constant, D is the magnetovolume coupling constant, and $M(T)$ is the magnetization. Equation (2) has also been widely used to uncover the characteristics and the mechanism of the MVEs in Invar-type alloys, such as Fe-Pt alloys [51,52], Fe-Ni alloys, and other $3d$ transition-metal alloys [53]. In 1980, Moriya and Usami also developed the same approximation as an ansatz in clarifying the mechanism of the magnetovolume effect in a magnetic system with spin fluctuations [54]. The $M(T)$ in Eq. (2) is always the macroscopic magnetization in the case of ferromagnetic NTE behaviors. Even in antiferromagnets, the $M(T)$ is also corresponding to the macroscopic magnetization obtained by the Curie-Weiss equation [48–50]. In the present case of antiperovskite compounds, due to the specific noncollinear nature of the magnetic structures, the macroscopic magnetization is not always corresponding to the spin magnetic structures and the volume variation [18] where Eq. (2) could not be used by the macroscopic magnetization as well. Furthermore, based on the good linear fit obtained by using the square of the magnetic moment m^2 for $Mn_3Ga_{1-x}Sn_xN$ compounds, as shown in Fig. 6(c) and the original theory of Eq. (2) [54], the microscopic electronic spin-ordered moment in the antiferromagnetic phase can be introduced to develop Eq. (2) as $\Delta\omega_m(T) = Cm^2(T)$, which could broaden its applicability to the typical antiferromagnetic MVE systems such as antiperovskites by generally assuming the bulk modulus B to be a constant. This is well justified since the bulk modulus generally has only a small relative change with temperature as compared with the magnetic moment [45].

Moreover, the magnetic free energy is given as [45]

$$\Delta F(T, \omega) = \phi(\omega) f(t(\omega)), \tag{3}$$

with $t(\omega) = T/T_0(\omega)$, where $T_0(\omega)$ is a critical temperature parameter and is assumed to be a linear function of ω [55]. $\phi(\omega)$ is the magnetic free energy in the ground state, which is sometimes referred to as the magnetic excitation potential and always depends on ω in the low-temperature region [45,47]. Near the Néel temperature, ϕ is assumed to be constant. Therefore, by assuming $f(t) = (1 - t^2)^2$ according to the Grüneisen-Testardi (GT) theory [47,56], one can obtain the equation [55,57]

$$\begin{aligned}\Delta\omega(T) &= -\frac{1}{B}\frac{\partial \Delta F}{\partial \omega} \\ &= -\frac{\emptyset'}{B}\left[1 + \left(4\frac{\emptyset}{\emptyset'}\frac{\partial ln T_0}{\partial \omega} - 2\right)\left(\frac{T}{T_0}\right)^2 \right. \\ &\quad \left. + \left(1 - 4\frac{\emptyset}{\emptyset'}\frac{\partial ln T_0}{\partial \omega}\right)\left(\frac{T}{T_0}\right)^4\right] \\ &= \Delta\omega(0)(1 + a_1T^2 + a_2T^4),\end{aligned} \tag{4}$$

where the parameters a_1 and a_2 contain ϕ, ϕ' and $\partial ln T_0/\partial\omega$. In order to deduce Eq. (4), the temperature dependence of the magnetization can be developed as [57,58]

$$m^2(T) = m^2(0)\left[1 + \frac{T^2}{{T_N}^2} + \cdots\right]. \tag{5}$$

Since the magnetovolume experimental data point to the existence of a significant T^4 term, the magnetic moments obtained by NPD can be well described using the equation

$$m^2(T) = m^2(0)\left[1 - \alpha\left(\frac{T}{T_N}\right)^2 + \xi\left(\frac{T}{T_N}\right)^4\right], \tag{6}$$

shown as the solid lines in Figs. 4(a)–4(c), which finally yields the required temperature dependence of the $\Delta\omega_m(T) = Cm^2(T)$. Consequently, the volume strain of Eq. (4) can also be rewritten as

$$\frac{\Delta\omega_m(T)}{\Delta\omega_m(0)} = 1 - A_1\left(\frac{T}{T_N}\right)^2 + A_2\left(\frac{T}{T_N}\right)^4. \tag{7}$$

Actually, since the magnetic contributions to the bulk modulus can be expressed from Eq. (3) as $\Delta B(T) = \frac{\partial^2 \Delta F}{\partial \omega^2}$, the magnetoelastic coupling constant $C(=D/B)$ should also be temperature dependent. Therefore, according to the equation $\Delta\omega_m(T) = C(T)m^2(T)$, the temperature variation of the magnetoelastic coupling constant is given as

$$C(T) = C(0)\left[1 - \gamma\left(\frac{T}{T_N}\right)^2\right], \tag{8}$$

which could also have an effect [50,59] on the importance of a fourth-degree term in $\Delta\omega_m(T)$. By using Eqs. (6) and (8), the magnetovolume reduces to

$$\Delta\omega(T) = C(0)m^2(0)\left[1 - (\alpha+\gamma)\left(\frac{T}{T_N}\right)^2 + (\xi+\alpha\gamma)\left(\frac{T}{T_N}\right)^4\right]. \quad (9)$$

Comparing with Eq. (7), there should exist several relationships between the parameters $A_1 = \alpha + \gamma$ and $A_2 = \xi + \alpha\gamma$, which induce a constraint of $A_2 = \alpha A_1 + \xi - \alpha^2$ when fitting the experimental data using Eq. (7), shown in Fig. 6(d). Table III gives all the fitting parameters in Eqs. (6)–(8) for $Mn_3Ga_{1-x}Sn_xN$ ($x = 0.1, 0.7, 0.9$) compounds. It can be seen that the value of the parameter C, treated as a constant in the equation $\Delta\omega_m(T) = C(T)m^2(T)$, is much close to the parameter $C(0)$ in Eq. (8), and the temperature parameter γ is also quite small, which is in agreement with the assumption in the fitting in Fig. 6(c). Therefore, the magnetovolume effect of $Mn_3Ga_{1-x}Sn_xN$ compounds can be well explained by these itinerant electron theories discussed above, which are widely used in antiperovskites.

IV. CONCLUSION

In conclusion, the magnetovolume effects in $Mn_3Ga_{1-x}Sn_xN$ compounds with Γ^{5g} magnetic structures were clarified using a detailed analysis of NPD data. The Sn element doping can efficiently increase the Néel temperature from 327 to 485 K, strengthen the phonon contribution to the thermal expansion, and decrease the dm/dT in the transition range, which lead to the broadening of the transition temperature from 12 to 96 K and change the NTE behavior (-139.3 ppm/K at $x = 0.1$) into a PTE behavior (11.2 ppm/K at $x = 0.9$). Furthermore, in these antiperovskite compounds, a new quantitative relationship between the square of the ordered magnetic moment and the volume variation is established to be $\Delta\omega_m(T) = Cm^2(T)$, which remains valid in the whole temperature domain of the Γ^{5g} AFM phases. Moreover, the equations describing the temperature dependences of the magnetovolume effect $\Delta\omega_m$ [Eq. (7)], magnetic moment m [Eq. (6)], and magnetoelastic coupling constant C [Eq. (8)] are first analyzed in antiperovskites according to the itinerant-electron theories. The results presented here can be further employed not only to tune the thermal expansion behavior, but also to understand the mechanism of the spin-lattice coupling in antiperovskite materials.

ACKNOWLEDGMENTS

We would like to acknowledge the scientific and technical support we received during the neutron powder diffraction experiments on the CRG-D1B (ILL) operated by the CNRS. This work has benefited from the financial support of the National Natural Science Foundation of China (NSFC) (Grants No. 51732001, No. 51472017, and No. 51572010), the JSPS KAKENHI Grants No. JP15K14133 and No. JP16H04501, and the Fundamental Research Funds for the Central Universities. K.S. thanks the China Scholarship Council (CSC) for scholarship support.

[1] J. R. Salvador, F. Guo, T. Hogan, and M. G. Kanatzidis, Nature (London) **425**, 702 (2003).
[2] T. A. Mary, J. S. O. Evans, T. Vogt, and A. W. Sleight, Science **272**, 90 (1996).
[3] B. K. Greve, K. L. Martin, P. L. Lee, P. J. Chupas, K. W. Chapman, and A. P. Wilkinson, J. Am. Chem. Soc. **132**, 15496 (2010).
[4] T. Kanomata, H. Ishigaki, T. Suzuki, H. Yoshida, S. Abe, and T. Kaneko, J. Magn. Magn. Mater. **140**, 131 (1995).
[5] M. Schilfgaarde, I. A. Abrikosov, and B. Johansson, Nature (London) **400**, 46 (1999).
[6] L. Dubrovinsky, N. Dubrovinskaia, I. A. Abrikosov, M. Vennström, F. Westman, S. Carlson, M. van Schilfgaarde, and B. Johansson, Phys. Rev. Lett. **86**, 4851 (2001).
[7] P. Álvarez-Alonso, P. Gorria, J. A. Blanco, J. Sánchez-Marcos, G. J. Cuello, I. Puente-Orench, J. A. Rodríguez-Velamazán, G. Garbarino, I. de Pedro, J. R. Fernández, and J. L. Sánchez Llamazares, Phys. Rev. B **86**, 184411 (2012).
[8] P. Gorria, P. Álvarez-Alonso, J. Sánchez-Marcosb, J. L. Sánchez Llamazaresa, M. J. Pérezav, and J. A. Blancoa, Acta Mater. **57**, 1724 (2009).
[9] Y. W. Long, N. Hayashi, T. Saito, M. Azuma, S. Muranaka, and Y. Shimakawa, Nature (London) **458**, 60 (2009).
[10] M. Azuma, W. Chen, H. Seki, M. Czapski, S. Olga, K. Oka, M. Mizumaki, T. Watanuki, N. Ishimatsu, N. Kawamura, S. Ishiwata, M. G. Tucker, Y. Shimakawa, and J. P. Attfield, Nat. Commun. **2**, 347 (2011).
[11] J. J. Neumeier, T. Tomita, M. Debessai, J. S. Schilling, P. W. Barnes, D. G. Hinks, and J. D. Jorgensen, Phys. Rev. B **72**, 220505 (2005).
[12] J. Chen, L. L. Fan, Y. Ren, Z. Pan, J. X. Deng, R. B. Yu, and X. R. Xing, Phys. Rev. Lett. **110**, 115901 (2013).
[13] J. Chen, X. R. Xing, C. Sun, P. H. Hu, R. B. Yu, X. W. Wang, and L. H. Li, J. Am. Chem. Soc. **130**, 1144 (2008).
[14] P. H. Hu, J. Chen, J. X. Deng, and X. R. Xing, J. Am. Chem. Soc. **132**, 1925 (2010).
[15] A. Say, O. Mys, A. Grabar, Y. Vysochanskii, and R. Vlokh, Phase Trans. **82**, 531 (2009).
[16] K. Takenaka and H. Takagi, Appl. Phys. Lett. **87**, 261902 (2005).
[17] X. Y. Song, Z. H. Sun, Q. Z. Huang, M. Rettenmayr, X. M. Liu, M. Seyring, G. N. Li, G. H. Rao, and F. X. Yin, Adv. Mater. **23**, 4690 (2011).
[18] S. H. Deng, Y. Sun, H. Wu, Q. Z. Huang, J. Yan, K. W. Shi, M. I. Malik, H. Q. Lu, L. Wang, R. J. Huang, L. F. Li, and C. Wang, Chem. Mater. **27**, 2495 (2015).
[19] Y. C. Wen, C. Wang, M. Nie, Y. Sun, L. H. Chu, and C. Dong, Appl. Phys. Lett. **96**, 041903 (2010).
[20] D. Matsunami, A. Fujita, K. Takenaka, and M. Kano, Nat. Mater. **14**, 73 (2015).

[21] K. W. Shi, Y. Sun, J. Yan, S. H. Deng, L. Wang, H. Wu, P. W. Hu, H. Q. Lu, M. I. Malik, Q. Z. Huang, and C. Wang, Adv. Mater. **28**, 3761 (2016).

[22] P. Lukashev, R. F. Sabirianov, and K. Belashchenko, Phys. Rev. B **78**, 184414 (2008).

[23] J. Yan, Y. Sun, H. Wu, Q. Z. Huang, C. Wang, Z. X. Shi, S. H. Deng, K. W. Shi, H. Q. Lu, and L. H. Chu, Acta Mater. **74**, 58 (2014).

[24] B. S. Wang, P. Tong, Y. P. Sun, L. J. Li, W. Tang, W. J. Lu, X. B. Zhu, Z. R. Yang, and W. H. Song, Appl. Phys. Lett. **95**, 222509 (2009).

[25] S. H. Deng, Y. Sun, L. Wang, H. Wu, K. W. Shi, P. W. Hu, Q. Z. Huang, and C. Wang, Appl. Phys. Lett. **108**, 041908 (2016).

[26] Y. S. Sun, Y. F. Guo, X. X. Wang, Y. Tsujimoto, Y. Matsushita, Y. G. Shi, C. Wang, A. A. Belik, and K. Yamaura, Appl. Phys. Lett. **100**, 161907 (2012)

[27] Y. Sun, Y. Guo, Y. Tsujimoto, J. Yang, B. Shen, W. Yi, Y. Matsushita, C. Wang, X. Wang, J. Li, C. I. Sathish, and K. Yamaura, Inorg. Chem. **52**, 800 (2013).

[28] J. Rodriguez-Carvajal, Phys. B **192**, 55 (1993).

[29] See Supplemental Material at http://link.aps.org/supplemental/10.1103/PhysRevB.97.054110 for room-temperature XRD (Fig. S-1) and XPD refinement plot (Fig. S-2), additional M-T data (Fig. S-3), and the difference plots of the NPD patterns (Fig. S-4).

[30] A. R. Denton and N. W. Ashcroft, Phys. Rev. A **43**, 3161 (1991).

[31] J. M. Perez-Mato, S. V. Gallego, E. S. Tasci, L. Elcoro, G. de la Flor, and M. I. Aroyo, Annu. Rev. Mater. Res. **45**, 13.1 (2015).

[32] D. Fruchart and E. F. Bertaut, J. Phys. Soc. Jpn. **44**, 781 (1978).

[33] K. Takenaka, T. Inagaki, and H. Takagi, Appl. Phys. Lett. **95**, 132508 (2009).

[34] T. Kiyama, K. Yoshimura, K. Kosuge, Y. Ikeda, and Y. Bando, Phys. Rev. B **54**, R756 (1996).

[35] R. Ranjan, A. Senyshyn, R. Garg, and H. Boysen, J. Appl. Phys. **109**, 073908 (2011).

[36] M. Blackman, Proc. Phys. Soc. (London) **74**, 17 (1959).

[37] F. Sayetat, P. Fertey, and M. Kessler, J. Appl. Cryst. **31**, 121 (1998).

[38] P. Fertey and F. Sayetat, J. Appl. Cryst. **29**, 692 (1996).

[39] M. R. Ibarra, P. A. Algarabel, C. Marquina, J. Blasco, and J. García, Phys. Rev. Lett. **75**, 3541 (1995).

[40] T. Taniguchi, S. Mizusaki, N. Okada, Y. Nagata, K. Mori, T. Wuernisha, T. Kamiyama, N. Hiraoka, M. Itou, Y. Sakurai, T. C. Ozawa, Y. Noro, and H. Samata, Phys. Rev. B **75**, 024414 (2007).

[41] V. Crisan, P. Entel, H. Ebert, H. Akai, D. D. Johnson, and J. B. Staunton, Phys. Rev. B **66**, 014416 (2002).

[42] F. Sayetat, J. X. Boucherle, and F. Tcheou, J. Magn. Magn. Mater. **46**, 219 (1984).

[43] K. Takenaka, M. Ichigo, T. Hamada, A. Ozawa, T. Shibayama, T. Inagaki, and K. Asano1, Sci. Technol. Adv. Mater. **15**, 015009 (2014).

[44] C. Wang, L. H. Chu, Q. R. Yao, Y. Sun, M. M. Wu, L. Ding, J. Yan, Y. Y. Na, W. H. Tang, G. N. Li, Q. Z. Huang, and J. W. Lynn, Phys. Rev. B **85**, 220103 (2012).

[45] E. Fawcett, H. L. Alberts, V. Y. Galkin, D. R. Noakes, and J. V. Yakhmi, Rev. Mod. Phys. **66**, 25 (1994).

[46] E. P. Wohlfarth, Solid State Commun. **35**, 797 (1980).

[47] S. G. Steinemann, J. Magn. Magn. Mater. **7**, 84 (1978).

[48] M. Hayase, M. Shiga, and Y. Nakamura, J. Phys. Soc. Jpn. **30**, 729 (1971).

[49] G. Hausch, Phys. Status Solidi A **41**, K35 (1977).

[50] H. L. Alberts and J. A. J. Lourens, Phys. Rev. B **29**, 5279 (1984).

[51] K. Sumiyama, M. Shiga, M. Morioka, and Y. Nakamura, J. Phys. F: Metal Phys. **9**, 1665 (1979).

[52] K. Sumiyama, M. Shiga, Y. Kobayahsi, K. Nishi, and Y. Nakamura, J. Phys. F: Metal Phys. **8**, 1281 (1978).

[53] M. Shiga, Solid State Commun. **10**, 1233 (1972).

[54] T. Moriya and K. Usami, Solid State Commun. **34**, 95 (1980).

[55] E. Fawcett, J. Phys.: Condens. Matter **1**, 203 (1989).

[56] S. G. Steinemann, J. Magn. Magn. Mater. **12**, 191 (1979).

[57] W. C. Muir, J. M. Perz, and E. Fawcett, J. Phys. F **17**, 2431 (1987).

[58] D. M. Edwards and E. P. Wohlfarth, Proc. R. Soc. London, Ser. A **303**, 127 (1968).

[59] A. Baran, H. L. Alberts, A. M. Strydom, and P. de V. du Plessis, Phys. Rev. B **45**, 10473 (1992).